Chapter 9
LD-Pumped Kilo-Joule-Class Solid-State Laser Technology

Takashi Sekine, Norio Kurita, and Toshiyuki Kawashima

Abstract In this chapter, we report our latest work on the technical development of the cryogenically cooled Yb:YAG-ceramics laser as scalable technology toward achievement of repetitive kilo-joule-class lasers. In our first trial, we obtain a high small signal gain of 20.4 with a high stored energy of 149.0 J using a conductively side-cooled Yb:YAG ceramic multi-disk laser amplifier operating at 100-K cooling temperature. In the second trial, we obtain 117-J nanosecond pulsed laser output with a cryogenic-helium-gas face-cooled Yb:YAG ceramic multi-disk laser amplifier. In this study, we obtain 42.3% energy-extraction efficiency from the energy stored in the Yb:YAG ceramic disks. We also determined the specifications of the face-cooled laser amplifier designed for repetitive operation by flowing helium gas on the end faces of the Yb:YAG ceramic disks. The feasibility of a practical design for kilo-joule-class diode pumped solid state lasers with a cryogenically cooled Yb:YAG ceramic disks was demonstrated by the developed high-gain and high-efficiency laser technologies.

9.1 Introduction

Since the first demonstration of laser oscillation in 1960 [1], laser technologies have been progressing rapidly. The most important characteristic of a laser is coherent control of the photons in the temporal, spatial, and spectral domains. Therefore, the progress in laser technologies can be seen as a history of pursuing optimal control in these domains. A nanosecond coherent optical pulse was demonstrated in the temporal domain by Q-switch technology in 1962 [2]. Furthermore, picosecond and

T. Sekine (✉) · N. Kurita · T. Kawashima
Central Research Laboratory, Industrial Development Center, Hamamatsu Photonics K.K., 1820 Kurematsu, Nishi-Ku, Hamamatsu City, Shizuoka 431-1202, Japan
e-mail: t-sekine@crl.hpk.co.jp

N. Kurita
e-mail: norio.kurita@hpk.co.jp

T. Kawashima
e-mail: kawasima@crl.hpk.co.jp

K. Yamanouchi et al. (eds.), *Progress in Ultrafast Intense Laser Science XVI*,
Topics in Applied Physics 141, https://doi.org/10.1007/978-3-030-75089-3_9

femtosecond laser pulses were observed using the mode-locked laser oscillators in 1966 [3–5]. By using the interaction between electron and an electric field generated by a femto-second laser pulse, an atto-second optical pulse generation was demonstrated using high-order harmonic generation in 2001 [6]. In the spatial domain, a mega-watt electric field at micrometer scale were generated by focusing spatially coherent photons from a transverse single-mode laser pulse onto the diffraction limit spot area. An electric-field intensity can be enhanced by increasing the laser-pulse energy by expanding the laser beam size and maintaining the spatial coherence to avoid an optical damage on the material surface. The National Ignition Facility (NIF) at Lawrence Livermore National Laboratory (USA) achieved the highest pulsed laser energy output of 16 kJ with transverse-single mode at 1053 nm wavelength with a beam size of 30 cm by 30 cm in 2012 [7, 8]. Their research made great contribution in the progress of the high power laser technologies, such as fabrication of the high quality optical materials, dielectric coatings with high damage threshold, and optical polish in high precision. A chirped pulse amplification (CPA) technique realized by coherence controlling technologies in the temporal, spatial, and spectral domains invented in 1985 [9] made a significant contribution to increasing the focused electric-field intensity beyond 10^{22} W/cm^2. In Europe, Extreme Light Infrastructure (ELI) laser facilities, including 10-PW laser systems based on the CPA technique, have been constructed to expand the application range of ultra-intense lasers [10].

With the dramatic progress in these laser technologies, the application range of lasers has widely expanded to optical communication, semiconductor lithography, material processing, laser ranging, laser scalpels, microscopes, and so on. For these applications to be practical, many types of lasers, such as gas, excimer, laser diode (LD), and solid-state have been developed. A diode-pumped solid-state laser (DPSSL) was described as "a renaissance in solid-state laser development" by Dr. R. L. Byer (Stanford University, U.S.A.) in 1988 [11], and has recently been widely used as a continuous-wave (CW) based fiber laser with kilo-watt class output in material processing. With the current industrial trends of Internet of Things and Industry 4.0, lasers are one of the most important technologies for constructing manufacturing systems. A pulsed DPSSL is suitable for optimizing the processing conditions of such systems due to the flexibility of its laser characteristics such as pulse duration (shape), repetition rate, pulse energy, and wavelength. Therefore, demand for pulsed laser processing of tempered glass, carbon fiber reinforced plastic (CFRP), and high-tensile steel is now growing.

Figure 9.1 shows the relationship between laser pulse energy and pulse repetition rate of typical laser systems in development or on the market. White plots denote flashlamp-pumped laser systems and black plots denote DPSSL systems. Flashlamp-pumped lasers with high pulse energy but a low repetition rate have long been used in scientific applications and have achieved many important results. However, DPSSLs with low pulse energy but high repetition rate have been developed for material-processing laser systems. From this background, a DPSSL with high pulse energy and high repetition rate is expected to create a new market in not only novel material processing but also scientific applications such as high energy physics, laser acceleration, attosecond generation, quantum beam generation, and inertial fusion

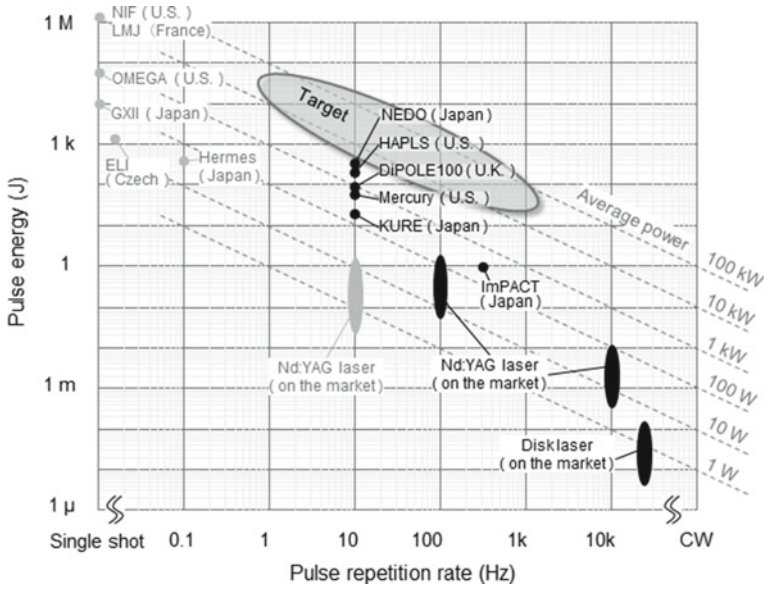

Fig. 9.1 Relationship between laser pulse energy and pulse repetition rate of typical laser systems in development or on the market

energy. Development of a high energy pulsed DPSSL began at the end of the 1990s in the U.S.A., Europe, and Japan. In 2007, 55 J at 10-Hz output from an LD-pumped Yb:S-FAP monocrystalline laser was achieve in the U.S.A. [12]. In 2008, 21.3 J at 10-Hz output was achieved from an LD-pumped Nd:glass laser in Japan [13]. In the latest report, 105 J at 10-Hz output was achieved using an LD-pumped cryogenically cooled Yb:YAG-ceramics laser in 2017 in the U.K. [14].

Since the 1990s, we have developed high-energy pulsed DPSSL technologies as fundamental research for the development of inertial fusion energy laser drivers. For a development of practical application in industrial and academic purposes, that must be processed for achieving our ultimate goal, we are developing high energy laser technology. Recently, such usage requires lasers of over 1-kW class average power in industrial fields; future applications in academic fields will require laser performance exceeding 10-kW average power. Therefore, in this chapter, we report our latest experimental results from the development of a cryogenically cooled Yb:YAG-ceramics laser amplifier as a feasibility study of kilo-joule-class lasers with a 10-Hz repetition rate [15].

9.2 Demonstration of High-Gain with High-Energy Storage Characteristics of Cryogenically Cooled Yb:YAG-Ceramics Laser Amplifier

In this section, we report a demonstration of high small-signal gain of 20 times along with high-energy storage characteristics of 149.0 J. This performance was achieved with an LD-pumped cryogenically side-cooled Yb:YAG ceramic multi-disk laser amplifier [16]. The results indicate the feasibility of developing practical kilo-joule class DPSSLs capable of simultaneously providing high gain as well as high-energy storage characteristics.

9.2.1 Construction of LD-Pumped Conductively Side-Cooled Yb:YAG Ceramic Multi-disk Laser Amplifier

The laser amplifier employed in this work uses Yb:YAG as a laser medium that can be adjusted to stimulated emission cross section suitable for high-energy lasers by cooling to a low temperature. Another advantage is that the established manufacturing technology of transparent Yb:YAG ceramics improves the reliability of high energy lasers. This multi-disk-type laser amplifier configuration is also suitable for a high energy laser amplifier due to its energy scalability made possible by enlarging the disk aperture. Such an amplifier can also be adapted to high-repetition operation by cooling the laser medium from the end-face with coolant. In the case of this laser amplifier, the Yb:YAG ceramic disks are conductively cooled from the side-surface via a copper holder using two Gifford-McMahon (GM) cryo-coolers. Thanks to this simple configuration of this amplifier, a high pulse energy extraction and high amplification gain is demonstrated. Consequently, the results from this amplifier allowed us to develop the cryogenic helium gas face-cooled Yb:YAG ceramic multi-disk laser amplifier discussed in this paper.

This LD-pumped Yb:YAG-ceramics laser amplifier was developed in 2015 by Hamamatsu Photonics K.K. (Fig. 9.2). Ten Yb:YAG ceramic disks, each with a size of 100 mm by 100 mm and a thickness of 10 mm, are placed in a central vacuumed laser chamber as the laser medium. Four LD modules are set around the vacuumed laser chamber. The LD modules pump the Yb:YAG ceramic disks from four diagonal directions. To prevent a difference in stored energy among the disks arranged at both ends and the center, we used five kinds of Yb:YAG ceramic disks with different Yb ion doping concentrations. Thus, lower concentration disks are arranged at both ends, and higher concentration disks are arranged at the center. The ten disks are cooled using two GM cryo-coolers installed in the upper and lower areas of the vacuumed laser chamber. The cooling capacity of the GM cryo-coolers is 180 W at 130 K. The side-surfaces of the Yb:YAG ceramic disks were treated to form a cladding layer for suppressing parasitic oscillation. Figure 9.3 shows a photograph of the Yb:YAG ceramic disks before cladding treatment. As shown by the arrow in Fig. 9.2, a seed

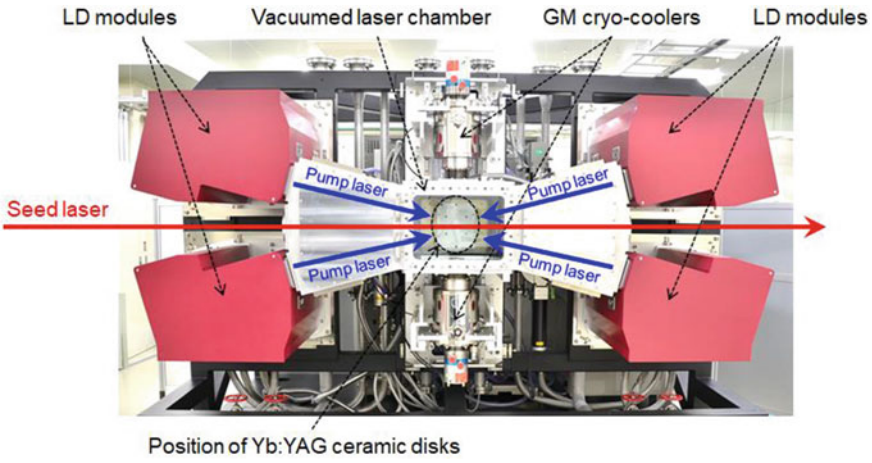

Fig. 9.2 Conductively cryogenic side-cooled Yb:YAG ceramic multi-disk laser amplifier

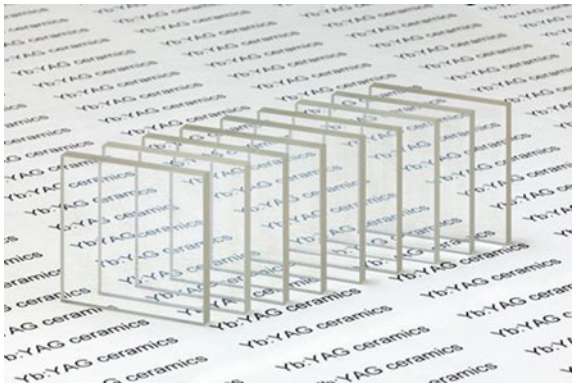

Fig. 9.3 Yb:YAG ceramic disks before cladding treatment

pulse propagates between the upper and lower LD modules and passes through the Yb:YAG ceramic disks after being injected into the vacuumed laser chamber from the vacuum window.

This laser amplifier is equipped with four water-cooled power supply systems for the four LD modules at the back. A total of 80 channels of electric pulse output are connected to each LD stack in the LD modules. The specifications of each output channel include a maximum output voltage of 60 V and maximum output current of 400 A with a pulse duration of 1 ms. Deionized water for the LD modules is supplied from a chiller with the capability of a 500-l/min flow rate with 0.8-MPa water pressure. All of the water is delivered through pipes from the rear-end of the system to cool the LD modules, LD power-suppling system, and GM cryo-coolers.

9.2.2 Characteristics of Pumping LD Modules

Table 9.1 gives the specifications of an LD stack used in the LD modules (shown by photo in Fig. 9.4). Jet-water-cooling LD stacks (model LE0115, Hamamatsu Photonics K.K.) are used. By driving a LD stack at 200-A current, it can output 6 J of energy with a peak power of 6 kW and a pulse duration of 1 ms. The typical repetition rate is 10 Hz. Thirty LD bars have cylindrical micro lenses for divergence collimation in the fast axis.

The specifications of an LD module are given in Table 9.2 (shown by photo in Fig. 9.5). An LD module outputs 110 kW in peak power. The typical irradiation size is 60 × 70 mm at a working distance of 700 mm. One of the unique characteristics of this LD module is that all output patterns from the LD stacks built into the LD module are superposed at the same position and in the same pattern at the working distance. This superposing scheme provides the averaging effects for the various intensities and the various spectrum of each LD stack. This scheme also has the advantage of avoiding spatial intensity defects in the irradiation pattern, even when a failure occurs in an LD stack.

A typical near-field pattern (NFP) at the working distance of an LD module is shown in Fig. 9.6. The intensity distribution in the NFP has a strong modulation at upper and lower areas. A number of vertically linear intensity distributions corresponding to the LD bars can also be confirmed. The intensity modulation at the upper and lower areas are explained from the aberration of the optical components used in the LD module. Another problem of the vertical-line profile is caused by the intensity

Table 9.1 Typical specifications of LD stack

Parameter	Value
Peak power	6 kW
Wavelength	940 nm
Pulse duration	1 ms
Repetition rate	10 Hz
Number of LD bars	30 bars

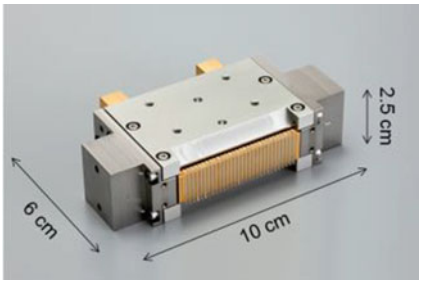

Fig. 9.4 Laser diode (LD) stack

Table 9.2 Typical specifications of LD module

Parameter	Value
Peak power	>110 kW
Wavelength	940 nm
Working distance	700 mm
Irradiation intensity	>2.6 kW/cm^2
Irradiation size (Rectangle)	60 × 70 mm

Fig. 9.5 LD module

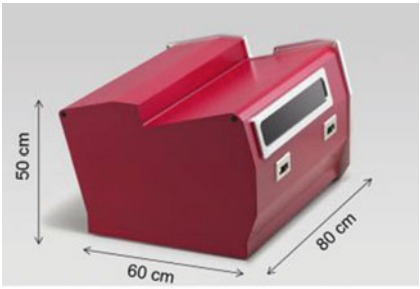

Fig. 9.6 Typical near-field pattern (NFP) of LD module

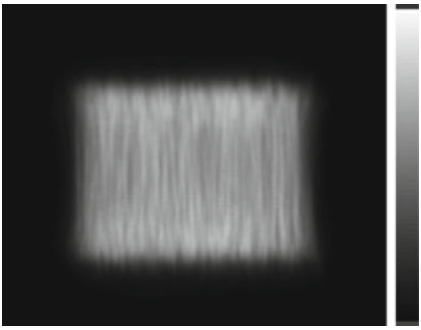

distribution of the LD bars. This pattern is expected to be improved by averaging with a four-direction pumping scheme.

9.2.3 Demonstration of High Small Signal Gain Characteristics with High-Energy Storage

Figure 9.7 shows a typical fluorescence pattern when Yb:YAG ceramic disks were pumped by four LD modules. The fluorescence pattern was measured in the horizontal direction along the same axis of the seed pulse path using a CMOS camera. The cooling temperature of the disks was 100 K, and the repetition rate of the LD

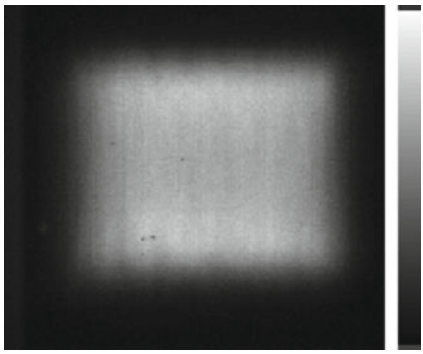

Fig. 9.7 Typical fluorescence pattern from Yb:YAG ceramics

modules was less than 1 Hz to avoid a temperature increase caused by pumping at a high repetition rate. The size of the fluorescent pattern was evaluated as 55 × 63 mm, and a smooth intensity profile in the pattern was observed. From the comparison between the fluorescent pattern (shown in Fig. 9.7) and a typical NFP of an LD module (shown in Fig. 9.6), the longitudinal line profile formed by the LD bars was clearly improved by the superposing effect of the four LD modules. However, strong upper and lower intensity distributions still remained. These distributions will be suppressed by optimizing the optical aberration management of the LD modules.

We conducted an experiment to evaluate the small-signal gain (SSG) characteristics of this laser amplifier. Generally, SSG can be expressed by the following formula.

$$G_0 = e^{\frac{E_{\mathrm{st}}\sigma_{\mathrm{em}}}{h\nu}\times l} = e^{\frac{E_{\mathrm{st}}}{E_s}l} = e^{g_0 l} \tag{1}$$

Here, G_0 is the SSG value, E_{st} is stored energy density, σ_{em} is the stimulated emission cross section, ν is oscillation frequency, c is the speed of light, h is the Planck constant, and l is gain length. In addition, Es is defined as a saturation fluence, and g_0 is defined as a SSG coefficient. In the experiment, a probe pulse with a wavelength of 1030 nm, pulse duration of about 100 ns, and pulse energy of about 1 μJ were input into this laser amplifier, and the amplification factor of the probe pulse with respect to the pump energy by the LD modules was measured. The cooling temperature of the Yb:YAG ceramic disks was 100 K, and the repetition rate of the pumping by the LD modules was less than 1 Hz. To suppress the temperature increase in the Yb:YAG ceramic disks caused by the pumping, the repetition rate was kept low.

The experimental results are shown in Fig. 9.8. The horizontal axis shows the pump energy, and the vertical axis shows the SSG values on a logarithmic scale. The SSG increases exponentially with respect to the stored energy, as represented by Eq. (1). A SSG of 20.4 times was obtained at 450.4-J pumping energy, and the energy stored inside Yb:YAG ceramic disks was calculated to be 149.0 J from Eq. (1) by assuming a pumped volume of 346.5 cm^3. These results show the feasibility of a laser amplifier with high stored energy as well as high gain using low-temperature-cooled Yb:YAG ceramics.

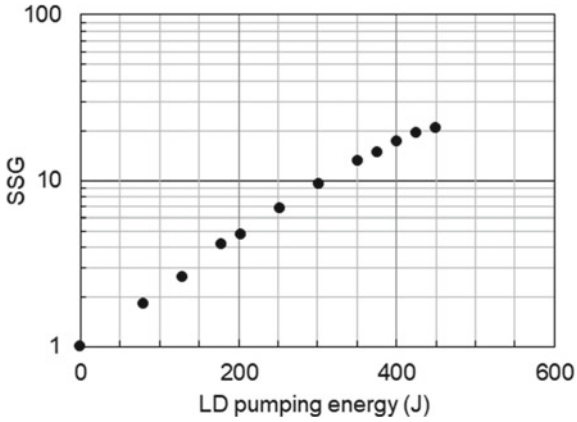

Fig. 9.8 Small-signal gain (SSG) characteristics

The $g_0 \times l$ (an index for generating unexpected oscillation (parasitic oscillation) in the laser medium) on the probe pulse propagation axis was evaluated to be about 3 from a SSG of 20.4 times. If $g_0 \times l$ exceeds 4, parasitic oscillation would start or the amplification of spontaneous emission (ASE) would significantly increase. From this estimation of $g_0 \times l$, the Yb:YAG ceramic disks exhibit a high SSG of 20.4 times while maintaining high stored energy of 149.0 J without parasitic oscillation. From Fig. 9.8, it was confirmed that the SSG showed good linearity in the logarithmic scale with respect to the pump energy up to 300 J; however, there was a tendency for this to gradually saturate over 300 J. The $g_0 \times l$ was calculated to be about 3.89 for 450.4-J pumping when the diagonal length in the three-dimensional pumping region in the Yb:YAG ceramic disks was used as the maximum gain length. Thus, it is assumed that the ASE inside the Yb:YAG ceramics significantly increases at over 300 J of pump energy.

9.2.4 Demonstration of 55.4 J Laser-Pulse Amplification

We conducted an energy-extraction experiment of this laser amplifier. An input pulse with a pulse duration of 20 ns and pulse energy of about 1 J was used. The seed pulse passed through the laser amplifier two times by constructing a pulse propagating system using an image-relaying telescope and a 0-degree reflection mirror. The experimental results of output energy with respect to the input energy are shown in Fig. 9.9. An output energy of 55.4 J was obtained when the input was 0.98 J. The solid line in Fig. 9.9 indicates the calculation results. The calculation code is based on the *Franz-Nodvik* equation model [17]. The stored energy estimated from the SSG measurement was used for the calculation. The results of the experiment were slightly lower than those of the calculation. The extraction efficiency was 36.5%, and the optical-to-optical conversion efficiency was 12.3%. The calculation results indicate that higher output energy could be expected due to the increased input energy.

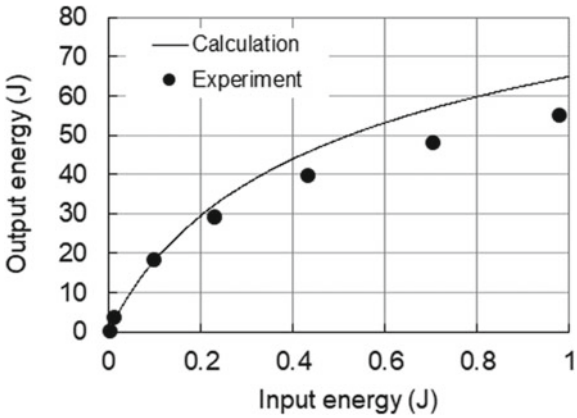

Fig. 9.9 Output energy characteristics as a function of input energy

The NFP of the output pulse is shown in Fig. 9.10. The pattern profile was similar to the fluorescent pattern shown in Fig. 9.7. Then the average fluence was evaluated to be 2.36 J/cm^2 with the pattern size of 46 $\times$ 51 mm.

In this section, we demonstrate high-energy laser amplification with high gain characteristics with an LD-pumped cryogenically cooled Yb:YAG ceramic multi-disk laser amplifier. This serves as a feasibility study of compact kilo-joule class DPSSLs.

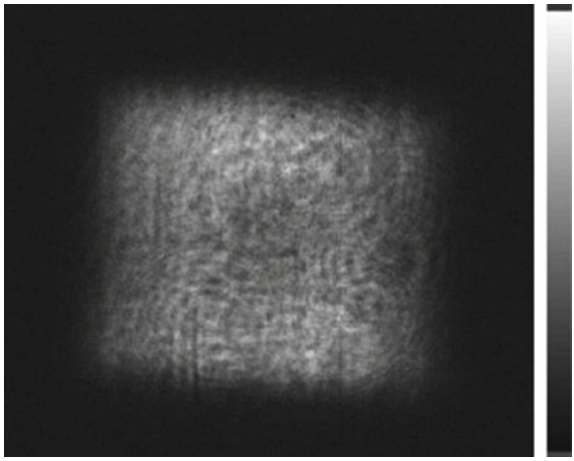

Fig. 9.10 NFP of 55-J output pulse

9.3 Demonstration of High-Energy Laser Output with High Energy-Extraction Efficiency Characteristics of Cryogenically Cooled Yb:YAG-Ceramics Laser Amplifier

In this section, we report a demonstration of 117 J laser output with over 40% energy-extraction efficiency using an LD-pumped cryogenic-helium-gas face-cooled Yb:YAG ceramic multi-disk laser amplifier [18]. The results indicate the feasibility of practical kilo-joule-class DPSSLs by demonstrating simultaneously high energy output and high-efficiency characteristics.

9.3.1 Construction of LD-Pumped Cryogenic-Helium-Gas Face-Cooled Yb:YAG Ceramic Multi-disk Laser Amplifier

A photograph of this amplifier is shown in Fig. 9.11, and its conceptual design is similar to the cryogenically side-cooled Yb:YAG ceramic laser amplifier discussed in Sect. 9.2. Four LD modules are located around a laser chamber as the pumping source. A seed pulse propagates between the upper and lower LD modules. Six Yb:YAG ceramic disks are placed in the center of the laser chamber. The disks are arranged with slight gaps to allow the helium gas to flow on each end-face. Helium gas characteristics can be controlled at a temperature of 150 K to 300 K and pressure of 0.5 MPa or less. Helium gas temperature is controlled with the flow rate of liquid nitrogen at the heat exchanger. The laser chamber has a two-layer structure with an inner high-pressure vessel for helium gas and an outer vacuum vessel for thermal

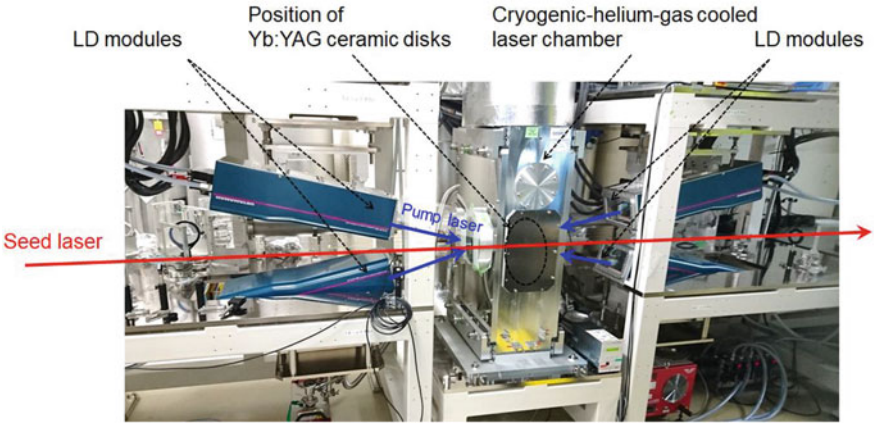

Fig. 9.11 Cryogenic-helium-gas face-cooled Yb:YAG ceramic multi-disk laser amplifier

insulation. Two sapphire windows joined on a metallic flange are attached to the high-pressure vessel as optical windows for delivering a seed pulse and four pump pulses into the Yb:YAG ceramic disks. A sapphire window requires extremely high sealing characteristics for low-temperature and high-pressure helium gas without causing leakage into the vacuum vessel. Cryogenic-helium-gas flows upward from the bottom of the laser chamber and then flows between the laser chamber and a cryogenic-helium-gas circulation device in a closed loop. The returned helium gas from the laser chamber is cooled by liquid nitrogen at the heat exchanger after being pumped up by the fan. The cooling capacity of the heat exchange is over 7 kW.

The size of a Yb:YAG ceramic disk in this amplifier is 120 mm in diameter by 10 mm in thickness and has a 7-mm-wide Cr:YAG ceramic cladding layer on the side-surface. These Yb:YAG ceramic disks and Cr:YAG ceramic layers are joined by sintering. Three types of Yb:YAG ceramic disks with different Yb ion-doping concentrations are arranged to average the stored energy distribution over all of the disks.

9.3.2 Characteristics of Pumping LD Modules

Table 9.3 gives the specifications of an LD stack used for an LD module (shown by photo in Fig. 9.12). For this LD module, a passive-cooled LD stack (LE0703MOD, Hamamatsu Photonics K.K.) was used. This LD stack can output a peak power of 7.5 kW at a driving current of 800 A. Then, output energy reaches 7.5 J at a pulse duration of 1 ms. The maximum repetition rate is 10 Hz due to passive cooling.

Table 9.3 Typical specifications of LD stack

Parameter	Value
Peak power	7.5 kW
Wavelength	940 nm
Pulse duration	1 ms
Repetition rate	10 Hz
Number of LD bars	10 bars

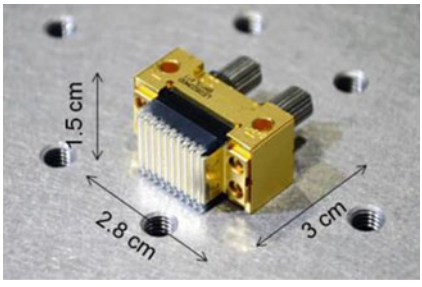

Fig. 9.12 LD stack

Table 9.4 Typical specifications of LD module

Parameter	Value
Peak power	>100 kW
Wavelength	940 nm
Repetition rate	10 Hz
Irradiation intensity	2 kW/cm^2
Irradiation size (Rectangle)	Adjustable between from 60 × 60 mm to 85 × 85 mm

Comparing this LD stack with that shown in Fig. 9.4, the output peak power of the LD bar is enhanced by more than three times, and the size of the LD stack is reduced to less than 1/10 while maintaining the same output energy.

The specifications of a pumping LD module are given in Table 9.4 (shown by photo in Fig. 9.13). The LD module can output over 100 J by operating at 100-kW peak power with a 1-ms-pulse duration. This LD module was designed using a superposing scheme of all LD stacks used in the LD module, the same as the pre-LD module shown Fig. 9.5. A unique characteristic of this LD module is that the rectangular irradiation pattern at the working distance of 560 mm can be changeable between from 60 × 60 mm to 85 × 85 mm by adjusting the internal optical system. The typical NFP of this LD module is shown in Fig. 9.14. The beam size is 85 × 72 mm. By optimizing the optical design, the uniformity of the intensity on the vertical-line shape profiles

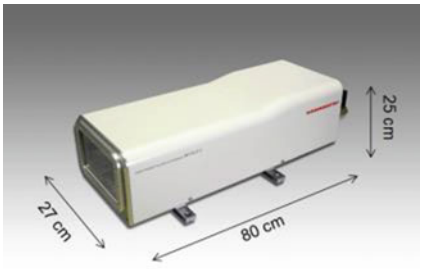

Fig. 9.13 LD module

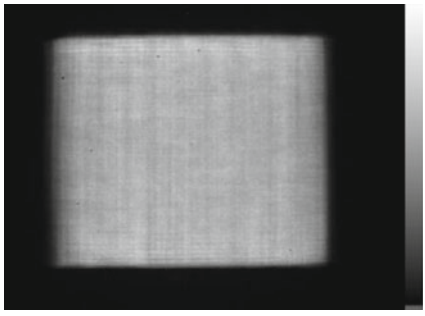

Fig. 9.14 Typical output NFP of LD module

and on the upper and lower distributions dramatically improved compared with the pattern measured in the previous works shown in Fig. 9.6.

9.3.3 *Characteristics of Small Signal Gain and Energy Extraction*

Figure 9.15 shows a typical fluorescence pattern of the Yb:YAG ceramic disks pumped by the LD modules from four direction in this laser amplifier. The cooling temperature of the Yb:YAG ceramic disks was 175 K, and the repetition rate of the LD modules was 1 Hz. A uniform and smooth pattern was obtained by improving the characteristics of the LD modules. The size of the fluorescent pattern was evaluated as 70.0 × 58.6 mm. The pumping intensity on the Yb:YAG ceramics was then evaluated as 2.7 kW/cm^2 for each LD module. It was also confirmed that flowing cryogenic-helium-gas had no effect on the fluorescent pattern on the Yb:YAG ceramic disks.

We measured the SSG characteristics of this laser amplifier. In this experiment, the cooling temperature of the Yb:YAG ceramic disks was 175 K, and the repetition rate of LD modules was 0.5 Hz. The experimental results are shown in Fig. 9.16. The horizontal axis shows the pump energy, and the vertical axis shows the SSG values on a logarithmic scale. A SSG of 4.5 times was confirmed at about 444.4-J pumping energy. The calculation results are shown with a solid line. The experimental results show good agreement with the calculation results up to 300 J. However, a slight deviation was observed over at 300 J. The ASE was much smaller than that in Fig. 9.8 because the SSG of this laser amplifier was around 4 times due to a higher cooling temperature of 175 K. One of the reasons for this saturation in SSG characteristics is assumed to be nonradiative loss in the Yb:YAG ceramics caused

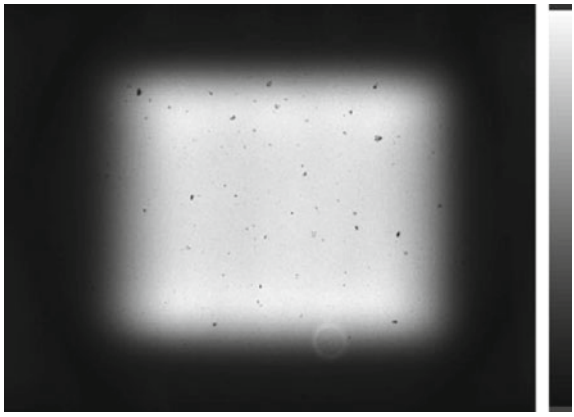

Fig. 9.15 Typical fluorescent pattern of Yb:YAG ceramics

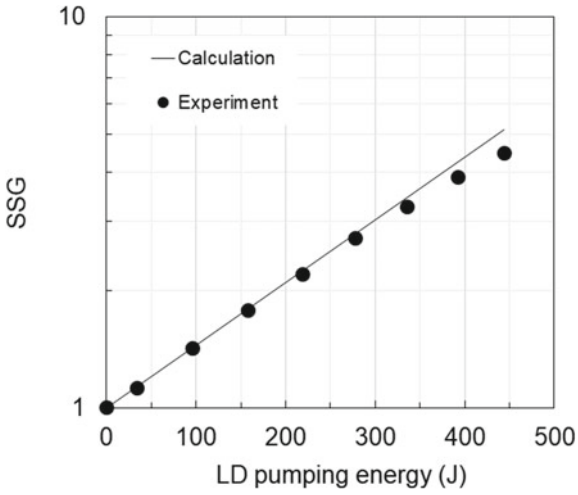

Fig. 9.16 SSG characteristics

by the Stokes shift and quantum efficiency. This nonradiative loss cause temperature increasing in the Yb:YAG ceramics.

We conducted an energy-extraction experiment using this laser amplifier. The input laser pulse had a pulse energy of 5 J, pulse duration of 40 ns in Gaussian shape, beam size of 7 × 7 cm, and pulse repetition rate of 0.05 Hz. We constructed an experimental set-up for single- and double-pass amplification. The seed pulse passed through the laser amplifier two times with different incident angles. The NFP at the first pass on the Yb:YAG ceramic disks was image-relayed to the ceramic disks in the second pass. The experimental results are shown in Fig. 9.17. The horizontal axis shows the pump energy by the LD modules, and the vertical axis shows the

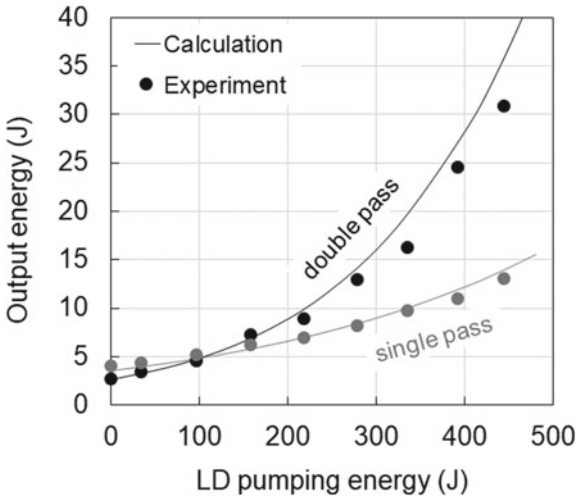

Fig. 9.17 Results of energy-extraction experiment

output energy of the laser amplifier. We obtained a 13.0 J output energy at single-pass amplification and 30.8 J at double-pass amplification. The pumping energy was 444 J. The calculation result simulated using the rate equation model is also shown with a solid line in Fig. 9.17. The calculation used the stored energy in the Yb:YAG ceramic disks estimated from the SSG experiment. The experimental results indicate good agreement with the calculation results, but there was a difference after exceeding a pump energy of 300 J. This difference can be explained by having the same characteristics as those estimated from the SSG experiment.

9.3.4 *Demonstration of 117-J Laser-Pulse Amplification with High Energy-Extraction Efficiency*

Figure 9.18 shows the configuration of a 100-J class high energy laser output demonstration using two cryogenic-helium-gas face-cooled Yb:YAG ceramic multi-disk laser amplifiers. These two laser amplifiers (laser heads 1 and 2) have a similar configuration in which six Yb:YAG ceramic disks are pumped by four LD modules from four directions. The maximum pump energy is 444 J for laser head 1 and 506 J for laser head 2. The pumping size on the Yb:YAG ceramic disks was 70.0 × 58.6 mm for laser head 1 and 75.4 × 58.9 mm for laser head 2. This experimental setup consisted of arranging the two laser heads, which have the double-pass amplification configuration, in series. The output pulse amplified by laser head 1 was input again to laser head 2 for double-pass amplification. An NFP and wave-front of the input pulse was relayed to the Yb:YAG ceramic disks in the two laser heads by

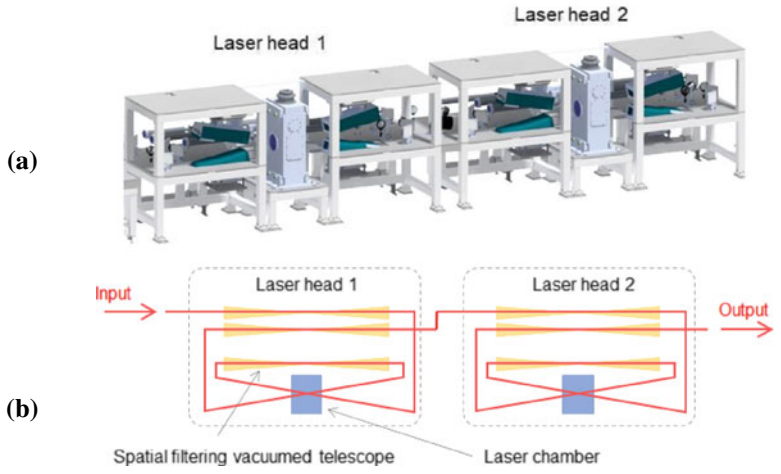

Fig. 9.18 Experimental setup for 100-J output demonstration. **a** 3D image of configuration. **b** Diagram of optical layout

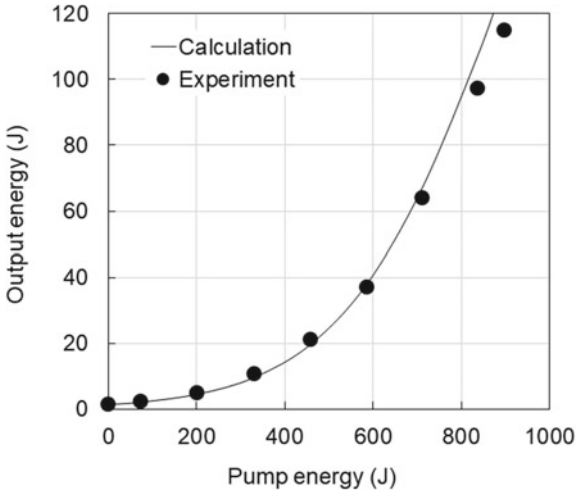

Fig. 9.19 Output energy characteristic

six vacuumed telescopes during every propagation. These telescopes also perform spatial filtering to prevent parasitic oscillation and straying laser pulses inside the two laser heads. The specifications of the input pulse for laser head 1 are the same as those from the SSG experiment for the single laser amplifier and energy extraction discussed in the previous section; the pulse energy was 5 J, pulse duration was 40 ns, and repetition rate was 0.05 Hz. In the experiment, the output energy after double-pass amplification of the two laser heads was measured by increasing the pump energy of the two laser heads simultaneously.

The output energy characteristics as a function of pump energy are shown in Fig. 9.19. A maximum output energy of 117 J was achieved at a total pump energy of 895 J in the two laser heads. The calculation results based on the rate-equation model are shown with a solid line. The optical-to-optical conversion efficiency was 12.5%. This calculation was conducted using actual characteristics of the pump energy and pumping area by the LD modules. In the calculation, pump efficiency defined by the ratio of the stored energy to pump energy was assumed to be 44% in both laser heads. This pump efficiency was evaluated from SSG measurement of laser head 1 as typical value. The experimental results indicate good agreement with the calculation results. The difference between the calculation and experiment results over 700 J is due to nonradiative transition in the Yb:YAG ceramics as in the SSG measurement. Energy extraction efficiencies of laser head 1 and 2 were evaluated as 13.4 and 42.3%, respectively. Here, the stored energies of the two laser heads of 171.3 and 210.5 J were evaluated by the multiplication of pump energy and pump efficiency of 0.44%.

An NFP of 117-J output is shown in Fig. 9.20. A smooth intensity profile without peak spots was confirmed. The smooth pumping profile obtained with four-direction pumping contributed to suppressing damage on the Yb:YAG ceramic disks. The intensity distributions at the upper and lower parts on the NFP are considered the effect of the pumping distribution, which has slight intensity modulation (Fig. 9.15).

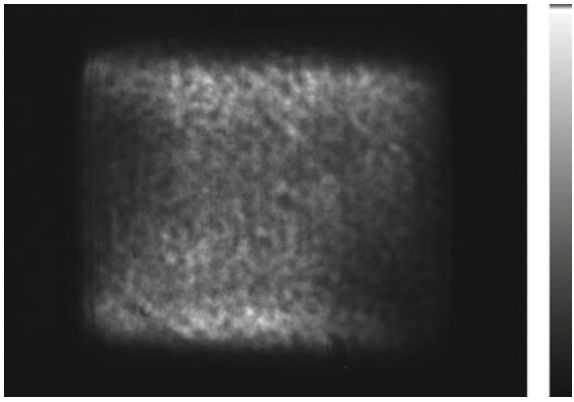

Fig. 9.20 NFP of 117 J output

The output pattern size is about 78 × 56 mm. Then the average fluence at the 117-J output is estimated to be about 2.68 J/cm^2. The reason for the dot-like profile on the NFP will be studied, along with the effect of the B-integral, in our future work.

In this section, we demonstrated high-energy laser amplification of over 100 J with high extraction-efficiency characteristics using an LD-pumped cryogenically cooled Yb:YAG ceramic multi-disk laser amplifier, thus providing a feasibility study of compact kilo-joule class DPSSLs.

9.4 Summary

In this chapter, we reported our current experimental results on cryogenically cooled Yb:YAG-ceramics laser amplifiers. This work was conducted as a feasibility study of kilo-joule class laser technologies. A high gain of 20.4 times with high stored energy of 149.0 J was demonstrated with a conductively side-cooled Yb:YAG ceramic multi-disk laser amplifier having a cooling temperature of 100 K. A 117-J output energy was also demonstrated with a cryogenic-helium-gas face-cooled Yb:YAG ceramic multi-disk laser amplifier having a cooling temperature of 175 K. Consequently, maximum efficiency as energy extraction was evaluated to be 42.3%. The demonstration of a high-gain laser amplifier while operating at a low temperature of about 100 K confirmed the feasibility of a compact and highly efficient design for kilo-joule-class DPSSLs.

We will develop fundamental laser technologies to demonstrate the high-energy and high-repetition capabilities made possible by using a cryogenic helium gas face-cooled Yb:YAG ceramic multi-disk laser amplifier. This further work will serve as a step toward achieving practical kilo-joule DPSSLs.

Acknowledgements A part of this report is based on the results obtained from a project commissioned by the New Energy and Industrial Technology Development Organization (NEDO), Japan.

References

1. T.H. Mainman, Nature **187**, 493 (1960)
2. F.J. McClung, R.W. Hellwarth, J. Appl. Phys. **33**, 828 (1962)
3. H.W. Mocker, R.J. Collins, Appl. Phys. Lett. **7**, 270 (1965)
4. A.J. DeMaria, D.A. Stetser, H. Heynau, Appl. Phys. Lett. **8**, 174 (1966)
5. D.A. Stetser, A.J. DeMaria, App. Phys. Lett. **9**, 118 (1966)
6. M. Hentschel, R. Kienberger, C. Spielmann, G.A. Reider, N. Milosevic, T. Brabec, P. Corkum, U. Heinzmann, M. Drescher, F. Krausz, Nature **414**, 509 (2001)
7. G. Brumfiel, Nature **491**, 170 (2012)
8. O.A. Hurricane, D.A. Callahan, D.T. Casey, P.M. Celliers, C. Cerjan, E.L. Dewald, T.R. Dittrich, T. Döppner, D.E. Hinkel, L.F. Berzak Hopkins, J.L. Kline, S. Le Pape, T. Ma, A.G. MacPhee, J.L. Milovich, A. Pak, H.-S. Park, P.K. Patel, B.A. Remington, J.D. Salmonson, P.T. Springer, R. Tommasini, Nature **506**, 343 (2014)
9. D. Strickland, G. Mourou, Opt. Commun. **56**, 291 (1985)
10. S. Wills, Opt. Photonics News **31**, 30 (2020)
11. R.L. Byer, Science **239**, 742 (1988)
12. A. Bayramian, P. Armstrong, E. Ault, R. Beach, C. Bibeau, J. Caird, R. Campbell, B. Chai, J. Dawson, C. Ebbers, A. Erlandson, Y. Fei, B. Freitas, R. Kent, Z. Liao, T. Ladran, J. Menapace, B. Molander, S. Payne, N. Peterson, M. Randles, K. Schaffers, S. Sutton, J. Tassano, S. Telford, E. Utterback, Fusion Sci. **52**, 383 (2007)
13. R. Yasuhara, T. Kawashima, T. Sekine, T. Kurita, T. Ikegawa, O. Matsumoto, M. Miyamoto, H. Kan, H. Yoshida, J. Kawanaka, M. Nakatsuka, N. Miyanaga, Y. Izawa, T. Kanabe, Opt. Lett. **33**, 1711 (2008)
14. P. Mason, M. Divoky, K. Ertel, J. Pilar, T. Butcher, M. Manus, S. Banerjee, J. Phillips, J. Smith, M.D. Vido, A. Lucianetti, C. Hernandez-Gomez, C. Edwards, T. Mocek, J. Collier, Optica **4**, 438 (2017)
15. http://www.nedo.go.jp/koubo/CD3_100053.html
16. T. Sekine, Y. Takeuchi, T. Kurita, Y. Hatano, Y. Muramatsu, Y. Mizuta, Y. Kabeya, Y. Tamaoki, Y. Kato, Proc. SPIE **10082**, 100820U (2017)
17. L.M. Frantz, J.S. Nodvik, J. Appl. Phys. **34**, 2346 (1963)
18. T. Sekine, T. Kurita, M. Kurata, Y. Hatano, Y. Muramatsu, T. Morita, Y. Kabeya, T. Iguchi, T. Watari, R. Yoshimura, Y. Tamaoki, Y. Takeuchi, Y. Mizuta, K. Kawai, Y. Zheng, Y. Kato, T. Suzuki, N. Kurita, T. Kawashima, S. Tokita, J. Kawanaka, N. Ozaki, Y. Hironaka, K. Shigemori, R. Kodama, R. Kuroda, E. Miura, submitted to High Energy Density Physics